Integrative Approaches to the Archaeology and History of Kültepe-Kaneš

© BREPOLS PUBLISHERS
THIS DOCUMENT MAY BE PRINTED FOR PRIVATE USE ONLY.
IT MAY NOT BE DISTRIBUTED WITHOUT PERMISSION OF THE PUBLISHER.

SUBARTU XLV

Subartu — a peer-reviewed series — is edited by the European Centre for Upper Mesopotamian Studies.

General Editor

Marc Lebeau

Editorial Board

M. Conceição Lopes
Lucio Milano
Adelheid Otto
Walther Sallaberger
Véronique Van der Stede

With the support of the following institutions

Università Ca' Foscari Venezia
Université Libre de Bruxelles
Universidade de Coimbra
Ludwig-Maximilians-Universität München

Subartu is a part of The East Collection

Cover image: Alabaster idol, EBA III, Kültepe mound, Kayseri Museum. H: 20.2 cm.
Photo: Murat Ertuğrul Gülyaz.

VOLUME 45

Previously published volumes in this series are listed at the back of the book.

© BREPOLS PUBLISHERS
THIS DOCUMENT MAY BE PRINTED FOR PRIVATE USE ONLY.
IT MAY NOT BE DISTRIBUTED WITHOUT PERMISSION OF THE PUBLISHER.

Integrative Approaches to the Archaeology and History of Kültepe-Kaneš

Kültepe, 4–7 August, 2017

Edited by

Fikri Kulakoğlu, Cécile Michel
& Güzel Öztürk

KIM Editors
Fikri Kulakoğlu & Cécile Michel

KIM Editorial Board
Levent Atici, Gojko Barjamovic, Guido Kryszat & Aslıhan Yener

KIM 3 — KÜLTEPE INTERNATIONAL MEETINGS 3

BREPOLS

© BREPOLS PUBLISHERS
THIS DOCUMENT MAY BE PRINTED FOR PRIVATE USE ONLY.
IT MAY NOT BE DISTRIBUTED WITHOUT PERMISSION OF THE PUBLISHER.

British Library Cataloguing in Publication Data

A catalogue record for this book is available from the British Library.

Keywords: Kültepe/Kaneš, Central Anatolia, Old Assyrian, Bronze Age, Near East, Trade, Glyptic, Clay Envelopes, Metallurgy, Turkey, Syria, Iraq.

© 2020, Brepols Publishers n.v., Turnhout, Belgium

All rights reserved. No part of this publication may be reproduced, stored in a retrieval system, or transmitted, in any form or by any means, electronic, mechanical, photocopying, recording, or otherwise, without the prior permission of the publisher.

D/2020/0095/152
ISBN: 978-2-503-58559-8
ISSN: 1780-3233

Printed in the EU on acid-free paper

© BREPOLS PUBLISHERS
THIS DOCUMENT MAY BE PRINTED FOR PRIVATE USE ONLY.
IT MAY NOT BE DISTRIBUTED WITHOUT PERMISSION OF THE PUBLISHER.

To

Mogens Larsen

on the Occasion of his Eightieth Birthday

Mogens Larsen, at Ankara Museum of Anatolian Civilizations, March 2016.
© Vanessa Tubiana-Brun.

© BREPOLS PUBLISHERS
THIS DOCUMENT MAY BE PRINTED FOR PRIVATE USE ONLY.
IT MAY NOT BE DISTRIBUTED WITHOUT PERMISSION OF THE PUBLISHER.

The 3rd Kültepe International Meeting took place the very year Mogens Larsen turned eighty. We wish to dedicate the proceedings of KIM 3 to Mogens as a token of friendship, and for his outstanding contribution to Old Assyrian studies.[1] If the Old Assyrian Text Project (OATP) was founded in Leiden in 1999, it really became efficient at the beginning of the twenty-first century when Mogens convinced the Carlsberg Foundation to support the project for twelve years. Copenhagen became the centre of the OATP, where Mogens built up a great team of young scholars dedicating all their time to the Old Assyrian period. Within the OATP, five PhDs were defended in Copenhagen, and these young colleagues were able to extend their researches through postdoctoral fellowships.[2] The OATP group met at least once a year in the city of Carsten Niebuhr, discussing topics and texts, exchanging data, dinners, and drinks. Last but not least, Mogens has published one of the largest Kültepe archive, making available in a few years more than 1200 new texts (AKT 6, *The Archive of Šalim-Aššur's Family*). Old Assyrian studies owe a lot to Mogens!

Fikri Kulakoğlu & Cécile Michel

[1] Mogens Larsen was presented a Festschrift in 2004: Jan Gerrit Dercksen (ed.), *Assyria and Beyond: Studies Presented to Mogens Trolle Larsen* (PIHANS C). Nederlands Instituut Voor Het Nabije Oosten, Leiden.

[2] The topics were varied: Karen Jensen, 'Marriage and Divorce in the Old Babylonian and the Old Assyrian Periods' (2003); Gojko Barjamovic, 'A Historical Geography of Ancient Anatolia in the Assyrian Colony Period' (2005); Thomas K. Hertel, 'Old Assyrian Legal Practices' (2008); Agnete W. Lassen, 'Glyptic Encounters: A Stylistic and Prosopographical Study of Seals in the Old Assyrian Period – Chronology, Ownership and Identity' (2012); Xiaowen Shi, 'Anatolians as Seen through the Old Assyrian Texts' (2013). Another PhD thesis defended in Chicago benefited from a year fellowship at Copenhagen, within the OATP: Edward P. Stratford, 'Archives, Agents, and Risk: An Account of Assyrian Commerce in 1894 BC' (2010).

© BREPOLS PUBLISHERS
THIS DOCUMENT MAY BE PRINTED FOR PRIVATE USE ONLY.
IT MAY NOT BE DISTRIBUTED WITHOUT PERMISSION OF THE PUBLISHER.

Contents

List of Illustrations xi
Acknowledgements xix

CÉCILE MICHEL

1. Integrative Approaches to the Archaeology and the History of Kültepe/Kaneš 1

New Approaches to Kültepe Archaeology and its Environment

FIKRI KULAKOĞLU, RYOICHI KONTANI, AKINORI UESUGI, YUJI YAMAGUCHI, KAZUYA SHIMOGAMA & MASAO SEMMOTO

2. Preliminary Report of Excavations in the Northern Sector of Kültepe 2015–2017 9
- Stratigraphy and Chronology 9
- Classification of Ceramics 16
- Remains Unearthed in Excavation Trench 1 21
- Excavation Trench 2 71
- Ceramic Sequence in the Northern Sector 71
- Tentative Conclusion and Future Perspectives 84

FIKRI KULAKOĞLU, SERDAR OKUR, GÜZEL ÖZTÜRK, GÖKHAN YILDIZ & DILEK KEÇE

3. Preliminary Report on the 2014–2016 Season Rescue Excavations at the Early Bronze Age Cemetery in Kayseri İnler Dağı 89
- Location of İnler Dağı Cemetery and Illegal Excavations 89
- Field Survey and Rescue Excavations 90

PINAR ERTEPINAR, COR LANGEREIS, ANDY BIGGIN, LENNART V. DE GROOT & FIKRI KULAKOGLU

4. Archaeomagnetism at Kültepe: Untangling the Order of Fire Events in Antiquity 99
- Introduction 99
- Background Information on Geo/Archaeo Magnetism 99
- Sampling 101
- Rock Magnetism 101
- Demagnetization, ChRM, and Directional Results 103
- Archaeointensity Experiments and Results 105
- Discussion 107
- Conclusions 110

THIS DOCUMENT MAY BE PRINTED FOR PRIVATE USE ONLY.
IT MAY NOT BE DISTRIBUTED WITHOUT PERMISSION OF THE PUBLISHER.

Natural Resources and their Exploitation

ANDREW FAIRBAIRN

5. Did the Old Assyrian Trade Stimulate Changes in Farming Practices in Central Anatolia? 115
A Short History of Farming in Central Anatolia 115
Did the Assyrian Trade Have an Identifiable Effect on Farming? 116
Discussion and Conclusion 118

ÇETIN ŞENKUL, FIKRI KULAKOĞLU, AZIZ ÖREN & WARREN EASTWOOD

6. Paleo-Ecological Conditions of Kültepe and its Vicinity Based on Palynological Data 123
Study Area and Geographical Features 125
The Palynological Approach in Investigation Methods 125
The Results of Analysis 126
Discussion and Conclusions 130

GONCA DARDENIZ & TAYFUN YILDIRIM

7. Resuloğlu (Çorum, Turkey) Updated: Preliminary Results of pXRF Analysis of Metal Artefacts from the Early Bronze Age Cemetery 141
Archaeological Context and Research Questions 143
Methodology and Results 144
Results 146
Discussion 152

ABDULLAH HACAR

8. Early Bronze Age Pottery from a Mining Settlement (Göltepe) South-West of Kültepe ... 163
Description of the Study Area 163
Early Bronze Age Pottery 164
Discussion 171

© BREPOLS PUBLISHERS
THIS DOCUMENT MAY BE PRINTED FOR PRIVATE USE ONLY.
IT MAY NOT BE DISTRIBUTED WITHOUT PERMISSION OF THE PUBLISHER.

From Object to Text — Kültepe History

EMINE KOÇAK & LATIF ÖZEN

9. Re-Restoring a Bone Panel from Kültepe-Kanesh 177
Condition of the Panel *in situ*/before Conservation 177
Condition before Conservation Treatment, Earlier Interventions, Deterioration, Physical and Chemical Decay 177
The Large Bones, U-Shaped and in the Form of a Trough 179
Lower and Upper Bone Plates on the Short Side of the Frame 179
Decorative Strips that Filled the Inside of the Frame 179
Restoration and Conservation Treatments 179
Choosing Cleaning Methodology 179
Location of Pieces and Reassembly of Groups 181
Reconstruction 182
Evaluation and Conclusion 185

CÉCILE MICHEL

10. Making Clay Envelopes in the Old Assyrian Period 187
Encasing a Tablet in the Old Assyrian Texts 187
The Envelopes in the '1993 Archive' 190
The Materiality of Envelopes and Envelope Fragments 191
Experimentation: How Were Envelopes Shaped? 199

MELISSA RICETTI

11. Preliminary Results on the Seal Impressions from the 1990 Excavation Season at Kültepe/Kaniš (kt 90/k) 205
Documents from the Kültepe 1990 Excavation Season 206
The Archive of Šumī-abīya and Aššur-mūtappil 207
Envelopes and Envelope Fragments in TPAK 1 208
Seals Impressed on TPAK 1 Envelopes: Style, Chronology, and Owners 210
The Identification of Seals and Sealers 216
Identified Seals: A Special Case 219

SELIM FERRUH ADALI

12. Iron Age Kültepe and its Region in Light of Tabal's History 225
Insights from the Scribes of Shalmaneser III and Tiglath-pileser III 225
The Kültepe Region from Wasusarma to Mugallu 230

© BREPOLS PUBLISHERS
THIS DOCUMENT MAY BE PRINTED FOR PRIVATE USE ONLY.
IT MAY NOT BE DISTRIBUTED WITHOUT PERMISSION OF THE PUBLISHER.

Disseminating Kültepe

ELIF SURER, CEREN İNCI TÜRKBEN & H. ŞEBNEM DÜZGÜN

13. A Multifaceted Gaming Platform for Interactive Learning of Archaeology and Culture of Kültepe: Preliminary Results on the Gaming Prototype 241

Materials and Methods 242

Results 244

Discussion 246

Conclusion and Future Work 249

Appendix A — The Quantic Lab — Quantic Foundry Gamer Profile Section 1 Questions 250

Appendix B — System Usability Scale Questions 251

Appendix C — Extended Technology Acceptance Model Questions 252

© BREPOLS PUBLISHERS
THIS DOCUMENT MAY BE PRINTED FOR PRIVATE USE ONLY.
IT MAY NOT BE DISTRIBUTED WITHOUT PERMISSION OF THE PUBLISHER.

List of Illustrations

Figures

Mogens Larsen, at Ankara Museum of Anatolian Civilizations, March 2016. v

Figure 1.1. Participants at the 3rd Kültepe International Meeting, Kültepe. 3

Figure 2.1. Location of the excavation area. 8

Figure 2.2. Location of the trenches excavated. 8

Figure 2.3. Excavation trench and its surrounding area, from north-west. 9

Figure 2.4. Excavation Trench 1. 9

Figure 2.5. Cross-section recorded in the deep sounding at the north-east corner of Excavation Trench 1. 11

Figure 2.6. Calibration results of ^{14}C dates. 12

Figure 2.7. Diagram of structural levels. 13

Figure 2.8. Classification of pottery. 14

Figure 2.9. Classification of pots and bowls. 16

Figure 2.10. Measurement system of pottery. 17

Figure 2.11. Features unearthed in Level I. 18

Figure 2.12. Portable hearth unearthed in Level I. 18

Figure 2.13. Pottery from Level I. 20

Figure 2.14. Pottery from Level I. 22

Figure 2.15. Pottery from Level I. 23

Figure 2.16. Miscellaneous objects from Level I. 24

Figure 2.17. Plan of features unearthed in Level II. 25

Figure 2.18. Marble human figurine (Idol no. 1) *in situ* in Level II. 25

Figure 2.19. Pottery from Level II. 26

Figure 2.20. Marble human figurine (Idol no. 1) from Level II. 27

Figure 2.21. Plan of features unearthed in Level III. 28

Figure 2.22. Features unearthed in Level III. 29

Figure 2.23. Pottery from Stone alignment no. 1, Level III. 30

© BREPOLS PUBLISHERS
THIS PDF MAY BE PRINTED FOR PRIVATE USE ONLY.
IT MAY NOT BE DISTRIBUTED WITHOUT PERMISSION OF THE PUBLISHER.

Figure 2.24. Pottery from Pit no. 1, Level III. 30
Figure 2.25. Pottery from Pit no. 1, Level III. 31
Figure 2.26. Pottery from Pit no. 1, Level III. 32
Figure 2.27. Pottery from Pit no. 2, Level III. 33
Figure 2.28. Marble human figurine (Idol no. 2) unearthed near Stone alignment no. 1, Level III. 34
Figure 2.29. Asphalt intact on Idol no. 2. 34
Figure 2.30. Stereomicroscope photographs and the infrared absorption spectra after chloroform solubility test. 35
Figure 2.31. Miscellaneous objects from Level III. 36
Figure 2.32. Miscellaneous objects from Level III. 37
Figure 2.33. Plan of features unearthed in Level IV. 37
Figure 2.34. Features unearthed in Level IV. 38
Figure 2.35. Pottery from Structure no. 1, Level IV. 39
Figure 2.36. Pottery from Level IV. 40
Figure 2.37. Miscellaneous objects from Level IV. 41
Figure 2.38. Plan of features unearthed in Level V (Structure no. 2). 42
Figure 2.39. Pottery from Level V. 43
Figure 2.40. Miscellaneous objects from Level V. 44
Figure 2.41. Plan of features unearthed in Level VI. 44
Figure 2.42. Features unearthed in Level VI. 45
Figure 2.43. Pottery from Level VI. 46
Figure 2.44. Pottery from Level VI. 47
Figure 2.45. Pottery from Level VI. 48
Figure 2.46. Miscellaneous objects from Level VI. 49
Figure 2.47. Miscellaneous objects from Level VI. 50
Figure 2.48. Pit with a stone alignment and a capstone (Stone alignment no. 4) unearthed in Level VII. 51
Figure 2.49. Pottery from Level VII. 51
Figure 2.50. Plan of features unearthed in Levels VII and VIII. 52
Figure 2.51. Pottery from Level VIII. 53
Figure 2.52. Plan of features unearthed in Level IX. 54
Figure 2.53. Features unearthed in Level IX. 54

© BREPOLS PUBLISHERS
THIS DOCUMENT MAY BE PRINTED FOR PRIVATE USE ONLY.
IT MAY NOT BE DISTRIBUTED WITHOUT PERMISSION OF THE PUBLISHER

Figure 2.54. Pottery from Level IX. 55
Figure 2.55. Miscellaneous objects from Level IX. 56
Figure 2.56. Plan of features unearthed in Level X. 56
Figure 2.57. Features unearthed in Level X. 57
Figure 2.58. Pottery from Level X. 58
Figure 2.59. Pottery from Level X. 59
Figure 2.60. Miscellaneous objects from Level X. 60
Figure 2.61. Plan of features unearthed in Level XI. 61
Figure 2.62. Clay-plastered stone wall (Structure no. 8) unearthed in Level XI. 61
Figure 2.63. Pottery from Level XI. 62
Figure 2.64. Clay sealing from Level XI. 63
Figure 2.65. Plan of features unearthed in Level XII. 64
Figure 2.66. Pottery unearthed in Level XII. 64
Figure 2.67. Stone slab unearthed in Level XII. 64
Figure 2.68. Pottery from Level XII. 65
Figure 2.69. Pottery from Level XII. 66
Figure 2.70. Plan of features unearthed in Level XIV. 67
Figure 2.71. Pottery unearthed in Level XIV. 67
Figure 2.72. Obsidian debitage from Level XIV. 67
Figure 2.73. Pottery from Level XIV. 68
Figure 2.74. Plan of features unearthed in Level XV. 69
Figure 2.75. Clay-plastered stone wall (Structure no. 11) unearthed in Level XV. 69
Figure 2.76. Pottery from Level XV. 70
Figure 2.77. Flint blade from Level XV. 70
Figure 2.78. Features unearthed in Excavation Trench 2 (geo-referenced ortho image). 71
Figure 2.79. Stratigraphic occurrence of pots of Ceramic Group 1. 72
Figure 2.80. Stratigraphic occurrence of pots of Ceramic Group 1. 73
Figure 2.81. Stratigraphic occurrence of bowls of Ceramic Group 1. 75
Figure 2.82. Stratigraphic occurrence of bowls of Ceramic Group 1. 76
Figure 2.83. Stratigraphic occurrence of Ceramic Group 2. 78
Figure 2.84. RD (rim diameter) distribution of Ceramic Groups 1 and 2. 79

© CYPRUS PUBLISHERS
THIS DOCUMENT MAY BE PRINTED FOR PRIVATE USE ONLY.
IT MAY NOT BE DISTRIBUTED WITHOUT PERMISSION OF THE PUBLISHER.

Figure 2.85. Painted pottery (nos 1–15: Level I). 81

Figure 2.86. Painted pottery (nos 1: Level II, nos 2–3: Level III, no. 4: Level IV, nos 5–7: Level V, nos 8–12: Level VI, no. 13: Level VII; no. 14: Level X, no. 15: Level XI). 82

Figure 3.1. Location of İnler Dağı Graveyard and Kültepe. 90

Figure 3.2. General view of İnler Dağı Graveyard from the west. 90

Figure 3.3. After illegal excavations at the graveyard. 91

Figure 3.4. A grave excavated by the smugglers. 91

Figure 3.5. Fragments of pottery unearthed by the smugglers. 91

Figure 3.6. Traces of burials laid on the karstic stratum. 92

Figure 3.7. Burial jars closed with stones (2015/M23). 92

Figure 3.8. One of the largest burials (2014/M03). 93

Figure 3.9. Tankard (2014/M09) and a *depas* (2014/M16). 93

Figure 3.10. A 'Troian plate' (left upper) unearthed in 2014/M09. 93

Figure 3.11. Grave 2014/M16 with a skull and a *depas*. 93

Figure 3.12. A lead tube (shell case?) with a hole at the bottom unearthed in Grave 2014/M16. 93

Figure 3.13. Grave 2014/M19. 94

Figure 3.14. Grave 2014/M20. 94

Figure 3.15. 'Intermediate' style beak-mouthed pitcher unearthed in Grave 2014/M20. 95

Figure 3.16. Imported (?) 'simple ware' pitcher unearthed in Grave 2014/M20. 95

Figure 3.17. An alabaster figurine of a seated goddess unearthed in Grave 2014/20. 96

Figure 3.18. Single and double-headed alabaster idols unearthed in 2015/M23. 96

Figure 4.1. Sampling locations on an aerial photograph of Kültepe (top). 100

Figure 4.2. Rock magnetic properties representative of each building material. 102

Figure 4.3. Representative examples of demagnetization diagrams of each type of building material, equal area projections of the ChRM directions of all sets, and the examples of accepted and rejected plots from three different protocols adopted in the archaeointensity experiments. 104

Figure 4.4. Declination, inclination, and VADM distribution of Kültepe data points. 108

Figure 5.1. Frequency of main cereal species. 118

Figure 6.1. Geographical location map of the study area. 124

Figure 6.2. Age-depth profiles for Lake Engir (EG16–01) and Lake Tuzla (TZL16–01). 126

Figure 6.3. Summary pollen percent diagram for Lake Engir (EG16–01). 128

Figure 6.4. Summary pollen percent diagram for Lake Tuzla (TZL16–01). 131

© BREPOLS PUBLISHERS
THIS DOCUMENT MAY BE PRINTED FOR PRIVATE USE ONLY.
FOR ANY OTHER USE, PERMISSION MUST BE OBTAINED FROM THE PUBLISHER

Figure 6.5. Pollen percentage diagram of Engir Lake showing anthropogenic plant taxa. 133

Figure 7.1. Map showing selected ancient settlements and resource areas mentioned in the text. 142

Figure 7.2. Cemetery and settlement areas of Resuloğlu overlooking Delice Valley. 143

Figure 7.3. Stone earring 8625 coated with the gold-silver alloy a) top view showing the stone body b) side view showing the details of the gold-silver coating. 147

Figure 7.4. A couple of rings (8614). ring_1 was found as copper-silver-gold-antimony whereas ring_2 was an alloy of copper-silver-gold. 147

Figure 7.5. The graph shows the diversity of metals detected through the pXRF analysis. It lists the object types and number of objects in each group. 147

Figure 7.6. Distribution of arsenic and tin levels in the artefacts according to alloy types. 148

Figure 7.7. The bivariate plot of arsenic by tin. 148

Figure 7.8. Anklets 7414 and 7415. 148

Figure 7.9. Pins 7513 and 8616 showing different types of alloys at the heads and shafts. 149

Figure 8.1. Map of sites mentioned in the text. 162

Figure 8.2. Göltepe viewed from Kestel Mine. 162

Figure 8.3. Göltepe EBA Ib vessel types. 165

Figure 8.4. Göltepe EBA II vessel types. 166

Figure 8.5. Göltepe EBA II vessel types. 168

Figure 8.6. Göltepe EBA II vessel types. 169

Figure 8.7. The example of Göltepe ware groups. 170

Figure 9.1. *In-situ* condition. 176

Figure 9.2. Condition before conservation and the bone pieces classified. 178

Figure 9.3. Deteriorations. 180

Figure 9.4. Cleaning and detachment. 179

Figure 9.5. Reinforcement and locating. 181

Figure 9.6. Reproduction. 182

Figure 9.7. Reconstruction. 183

Figure 9.8. Condition after conservation. 184

Figure 10.1. Letter to Rabi-Aššur, Ataya, Puzur-Aššur, Šu-Ištar, Šamaš-abi, Anina, Amārum, and Tariša from Aššur-taklāku; Kt 93/k 526 (4 × 6.7 cm), left edge, obverse, and reverse. 192

Figure 10.2. Envelope of a letter from Ah-šalim to Ištar-bāni, Kurub-Ištar, and Hattiya. 192

Figure 10.3. Envelope of a loan contract belonging to Aššur-taklāku, the debtor is Kabašunuwa, son of Kēna-Aššur. 193

© BREPOLS PUBLISHERS
THIS PDF MAY BE USED FOR PERSONAL RESEARCH PURPOSES ONLY
IT MAY NOT BE DISTRIBUTED WITHOUT PERMISSION OF THE PUBLISHER.

Figure 10.4. a) Letter, Kt 93/k 239+217; b) Contract, Kt 93/k 945; c) Letter Kt 93/k 143. 194

Figure 10.5. Two seal impressions of Tariša's seal on the envelope Kt 93/k 372+380. 195

Figure 10.6. Contract, Kt 93k 215a. 196

Figure 10.7. Royal letter Kt 93/k 201+376+381. 196

Figure 10.8. Inside of envelope Kt 93/k 865. 196

Figure 10.9. Join between envelope fragments Kt 93/k 232+136+220. 197

Figure 10.10. Inside of the envelope Kt 93/k 843 with the negative imprint of a 'second page'; Kt 93/k 211: tablet and 'second page' preserved in their envelope; Kt 93/k 55+120+831+240: join between two envelope fragments, main tablet, and 'second page'. 197

Figure 10.11. Insides of envelope fragments. Kt 93/k 552, Kt 93/k 228, Kt 93/k 117, Kt 93/k 142. 198

Figure 10.12. Textile and fibre imprints on the inside of envelopes. Kt 93/k 373, Kt 93/k 223. 199

Figure 10.13. Fossilized textile on the edge of a tablet. Kt 94/k 487. 199

Figure 10.14. The different steps in the manufacture of an envelope. 200

Figure 11.1. Text types of TPAK 1 envelopes. 208

Figure 11.2. a) Half envelope of a letter sent by Aššur-bāni s. Iddin-abum, reverse (kt 90/k 197); b) cylinder seal of Aššur-bāni s. Iddin-abum (kt 90/k 98; c) half envelope of a letter sent by Abāya, reverse (kt 90/k 199); d) cylinder seal of Abāya (kt 90/k 199, seal A = CS 840). 210

Figure 11.3. Style categorization of seal impressions on TPAK 1 envelopes. 211

Figure 11.4. a) Cylinder seal in Old Babylonian style with later additions in Syro-Cappadocian style; b) cylinder seal in Syro-Cappadocian style with inscription panel erased and filled with Anatolian motifs. 212

Figure 11.5. Drawings by the author of cylinder seals. 215

Figure 11.6. Drawings by the author of cylinder seals. 217

Figure 11.7. Half envelope with the impressions of four different seals (kt 90/k 254a). 218

Figure 11.8. Aššur-muttabbil's family tree. 220

Figure 13.1. Initial 'Welcome' screen of the platform; Choosing the theme of the games. 242

Figure 13.2. Geography Puzzle game's information screen; Trade & Law game's initial screen. 243

Figure 13.3. Answers to Question no. 2 of the Gamer Profile questionnaire. 244

Figure 13.4. Answers to Question no. 3 of the Gamer Profile questionnaire. 244

Figure 13.5. Answers to Question no. 4 of the Gamer Profile questionnaire. 245

Figure 13.6. Answers to Question no. 5 of the Gamer Profile questionnaire. 245

Figure 13.7. Answers to Question no. 6 of the Gamer Profile questionnaire. 245

Figure 13.8. Answers to Question no. 7 of the Gamer Profile questionnaire. 245

© BREPOLS PUBLISHERS
THIS DOCUMENT MAY BE PRINTED FOR PRIVATE USE ONLY
IT MAY NOT BE DISTRIBUTED WITHOUT PERMISSION OF THE PUBLISHER.

Figure 13.9. System Usability Scale questionnaire results plotted using mean and standard deviation values. 245

Figure 13.10. Extended TAM questionnaire results plotted using mean and standard deviation values. 246

Figure 13.11. Answers and suggestions to the open questions of TAM questionnaire. 248

Tables

Table 1.1. Volumes dedicated to Kültepe/Kaneš and the Old Assyrian period published between 2001 and 2018. 4

Table 2.1. AMS ^{14}C dates. 10

Table 2.2. Classification of RD and NH/RD. 19

Table 4.1. Site details sampled for this study. 101

Table 4.2. Summary of directional results. 105

Table 4.3. The intensity results obtained from three protocols 107

Table 5.1. Economic species recorded in seed assemblages at Kültepe and Kaman-Kalehöyük. 117

Table 6.1. Historical and archaeological settlement chronology of Kültepe. 125

Table 6.2. Radiocarbon/AMS ^{14}C ages from Lake Engir and Lake Tuzla sediment cores. 127

Table 6.3. Summary seed data for Kültepe's upper and lower cities. 132

Table 7.1. pXRF results of the Resuloğlu metal artefacts. 145

Table 8.1. Göltepe EBA ware groups. 164

Table 8.2. Göltepe EBA vessel types. 164

Table 11.1. Documents excavated at Kültepe in 1990. 206

Table 11.2. Envelopes with known or still encased tablets. 209

Table 11.3. Envelopes with Anatolian sealers. 214

Table 11.4. Identification of sealers in Kt 90/k 254a–b. 218

Table 11.5. Identification procedures. 219

Table 13.1. Positive and negative statements of the System Usability Scale questionnaire. 246

Table 13.2. Extended Technology Acceptance Model questionnaire. 247

© BREPOLS PUBLISHERS
THIS DOCUMENT MAY BE PRINTED FOR PRIVATE USE ONLY.
IT MAY NOT BE DISTRIBUTED WITHOUT PERMISSION OF THE PUBLISHER.

4. Archaeomagnetism at Kültepe: Untangling the Order of Fire Events in Antiquity

Pinar Ertepinar*, Cor Langereis*, Andy Biggin**, Lennart V. de Groot* & Fikri Kulakoglu***

Introduction

Archaeomagnetism is the study of burnt or fired archaeological artefacts with the aim of determining short term variations in the Earth's magnetic field over the past thousands of years, also called the paleosecular variation (PSV). A second and ultimate outcome regarding the archaeological use of these studies is to provide a dating tool for the fire events once a good master curve for the region is constructed using the well-dated material. Commonly studied *in-situ* features include kilns, hearths, ovens, and fires for paleo directions and intensities while *ex-situ* artefacts like ceramics and tiles can be used for paleointensity studies only.

The characterization of PSV is particularly important for understanding the geodynamo behaviour of the Earth. Based on the archaeomagnetic and historical or well-dated lava flow measurements all around the world, a number of global field models have been developed. The most recent models are pfm9k.1b[1] and SHA. DIF.14k[2] and are now widely used, having a better resolution compared to the older models. However, there are local variations in the field that are not detected by global field models such as the intensity high over the Levant region that occurred around 1050–750 BC, recently described by Shaar[3] as the 'Levantine Iron Age Anomaly (LIAA)'. In addition, the present data for directions is mainly derived from the sites in Eastern Europe and that causes a bias in the field models. Although the existing data around Turkey and the global field models give a first approximation of the ancient field, the use of archaeomagnetism as a dating tool requires a well-established PSV curve for this large region.

The main objective of this study is to solve (partly) the timing and character of the demise of this settlement by comparing our archaeomagnetic results from different parts of the settlement. We will argue that the abandonment of the site was not the result of a single big catastrophic event and we conclude that the site must have been destroyed (burned) in various stages.

Background Information on Geo/Archaeo Magnetism

The magnetic field of the Earth changes continuously and non-uniformly through time and space. The recent behaviour of the field is well known from the observatories. The historical changes (approximately last four hundred years) are reconstructed from the navigational observations while older records (past thousands of years) are derived through archaeomagnetism.

Almost all kinds of earth materials have magnetic minerals in their composition capable of recording the Earth's magnetic field primarily during the deposition process of the rocks, and afterwards, if disturbed with an agent like underground water, fire, pressure, etc. This record is called the 'Natural Remanent Magnetization (NRM)' and can be measured by using magnetometers. The NRM is expressed by three components; declination, inclination (directions of the vector in the horizontal and vertical plane, respectively), and intensity (the magnitude of the vector). Obtaining directional results and intensities require different treatments. In archaeomagnetic studies, in general, directional analyses are more straightforward compared to intensities. The only condition for reliable directions is the availability of the *in-situ* materials. Archaeointensity experiments on the other hand, are more difficult and time-consuming.

* Utrecht University, Department of Earth Sciences, Paleomagnetic Laboratory Fort Hoofddijk, 3584 CD Utrecht/The Netherlands, P.Ertepinar@uu.nl, C. G.Langereis@uu.nl, L. V.degroot@uu.nl.

** University of Liverpool, School of Environmental Sciences, Oliver Lodge Laboratories, Geomagnetism Laboratory, Liverpool/UK, A.Biggin@liverpool.ac.uk.

*** Ankara University, Faculty of Language and History-Geography, Department of Protohistory and Ancient Near Eastern Archaeology, Turkey/Ankara, kulakoglu@yahoo.com.

[1] Nilsson *et al.* 2014.

[2] Pavon-Carrasco *et al.* 2014.

[3] Shaar *et al.* 2016.

© ARCHAEOLS PUBLICATIONS
THIS DOCUMENT MAY BE PRINTED FOR PRIVATE USE ONLY
IT MAY NOT BE DISTRIBUTED WITHOUT PERMISSION OF THE PUBLISHER

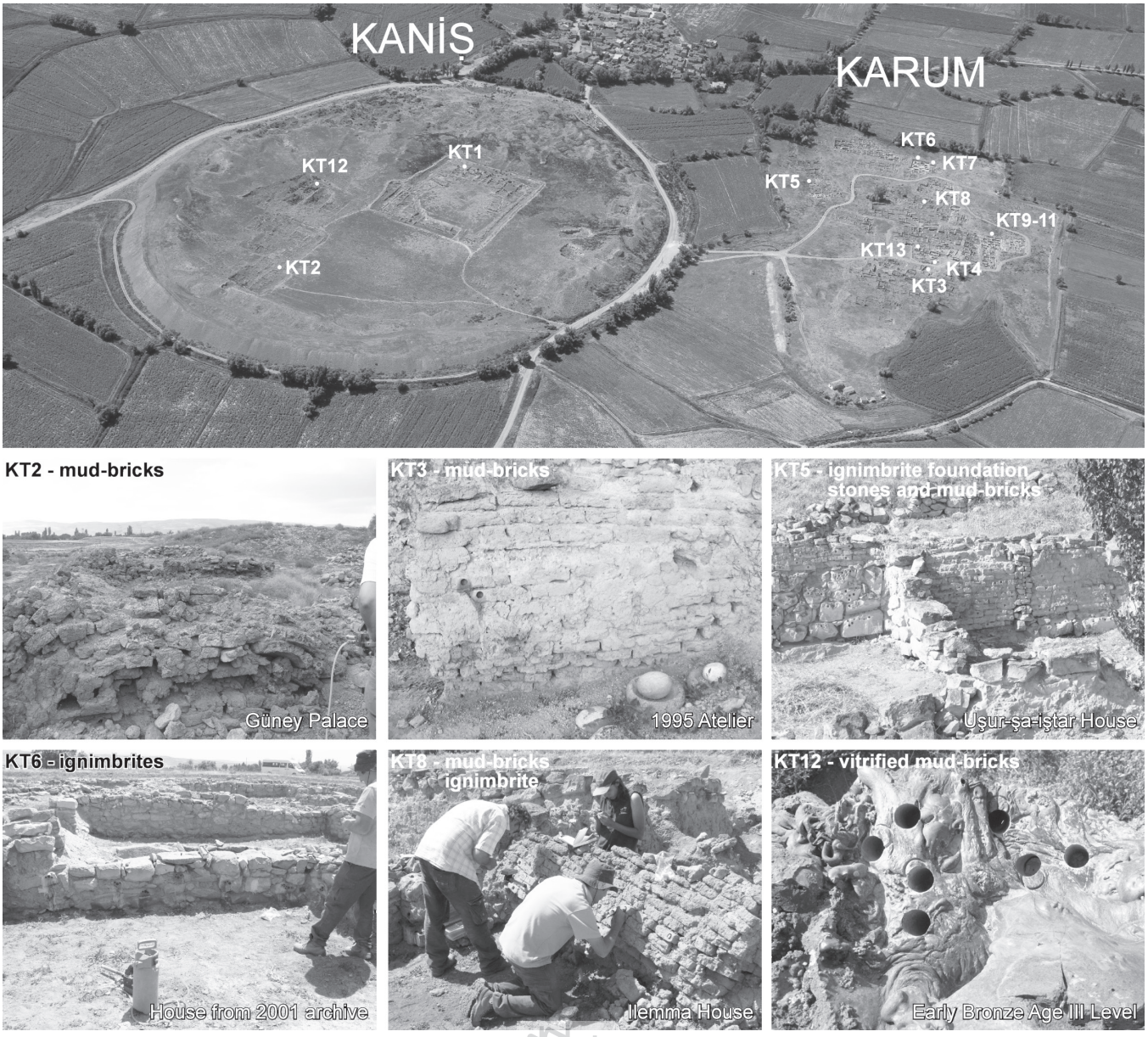

Figure 4.1. Sampling locations on an aerial photograph of Kültepe (top). Photographs show different building materials analysed in this study. Middle row from left to right: Güney Palace, 1995 Atelier, and Uşur-şa-iştar House. Bottom row from left to right: House from the 2001 Archive, Ilemma House, and Early Bronze Age III level (photo credit: Pinar Ertepinar, 20.06.2007 and 15.07.2008).

The success of the experiments is highly dependent on the material properties (explained in section 4) and the possible alteration of magnetic minerals — that can occur during repetitive heatings in the experimental procedure — also alters the results (whereas the directions are not significantly affected). There are additional problems, such as the anisotropy that can be introduced in the manufacturing process of archaeological artefacts, and the cooling rate effect caused by the time lag between actual and experiment cooling. Depending on the nature of the problem, all these effects should be monitored carefully prior, during, or after the experiment. Therefore, intensity experiments are more time consuming and have much lower success rate compared to obtaining directions.

Once all three components are well established from a fair number of well-dated data points covering a sequence of time intervals over a specified region (e.g. Turkey), it is possible to construct curves that define the magnetic field behaviour for that region that forms the basis for archaeomagnetic dating.

© SIDESTONE PUBLISHERS
THIS DOCUMENT MAY BE PRINTED FOR PERSONAL USE ONLY
IT MAY NOT BE DISTRIBUTED WITHOUT PERMISSION OF THE PUBLISHER

Table 4.1. Site details sampled for this study. Lat and Long are the coordinates of sampling sets (projection system: Latitude–Longitude, Datum: WGS 84) and N and N_{spec} are the number of samples and the total number of samples including the sister specimen. Table by the authors.

Site	Epoch	Lat (°N)	Long (°E)	Corresponding Kültepe-Karum level	Age (BCE)	Structure	Material	N	N_{spec}
Kültepe *(38°51'04"N, 35°38'69"E)*									
KT1	Middle Bronze	38.85139	35.63516	Kültepe-Karum Ib	1750±20	Warşama Palace	Mud-brick	25	34
KT2	Middle Bronze	38.84895	35.63471	Kültepe-Karum II	1850±20	Güney Palace	Mud-brick	34	54
KT3	Middle Bronze	38.85306	35.63946	Kültepe-Karum II	1892.5±57.5	1995 - atelier	Mud-brick	18	18
KT4	Middle Bronze	38.85324	35.63923	Kültepe-Karum II	1892.5±57.5	Selim Assur House	Mud-brick, ignimbrite	14	20
KT5	Middle Bronze	38.85379	35.63714	Kültepe-Karum II	1892.5±57.5	Uşur-şa-iştar House	Mud-brick, ignimbrite	46	74
KT6	Middle Bronze	38.85467	35.63739	Kültepe-Karum Ib	1765±65	House from 2001 archive	Ignimbrite	9	13
KT7	Middle Bronze	38.85470	35.63808	Kültepe-Karum Ib	1765±65	House with a mill	Ignimbrite	12	16
KT8	Middle Bronze	38.85415	35.63875	Kültepe-Karum II	1892.5±57.5	Ilemma House	Mud-brick, ignimbrite	14	20
KT9	Middle Bronze	38.85415	35.63977	Kültepe-Karum Ib	1765±65	House	Ignimbrite	21	34
KT10	Middle Bronze	38.85412	35.63977	Kültepe-Karum Ib	1765±65	House	Ignimbrite	7	13
KT11	Middle Bronze	38.85412	35.63977	Kültepe-Karum Ib	1765±65	House	Ignimbrite	9	16
KT12	Early Bronze III	38.85015	35.63360	—	2400±50	Mud-brick wall	Vitrified mud-brick	24	56
KT13	Middle Bronze	38.85342	35.63900	Kültepe-Karum II	1892.5±57.5	House	Mud-brick, ignimbrite	21	23

Sampling

For directional measurements, the sampling was done with a custom-made water-cooled drill to take oriented cylindrical cores of 2.5 cm diameter. Diamond drill bits and a non-magnetic orientation device were used to avoid magnetic contamination. Unoriented cores, pot sherds, and mud-brick fragments were sampled for archaeointensity experiments. For statistical confidence, we took at least seven samples (but generally more, up to forty-six) from each set, and we sampled as many different building materials as possible.

In the field season of 2007 and 2008, we collected thirteen sets of samples; three from the mound (the upper town) and ten sets from Kârum part (the lower town). Two of the mound sets, KT1 and KT2, are from Waršama Palace and Güney Palace, respectively, with corresponding Kârum levels of Ib and II. Both palaces were completely destroyed by intense fires. These sets are composed solely of mud-bricks. The third mound set (KT12) is from the vitrified mud-bricks of an Early Bronze Age level. The Kârum sets consist either solely of ignimbrites or of a combination of mud-bricks and ignimbrites. The mud-bricks in the settlement were used as building stones while the ignimbrites were used as foundation stones. All ten sets are from different rooms where five sets are from level Ib and the other five are from level II. The site is only a few kilometres away from a massive stratovolcano, and the types of ignimbrites used in the foundation show considerable variation. In some parts of the settlement, the fire was so intense that the mud-bricks were molten and became vitrified. The locations and the details of sampling sets are given in Figure 4.1 and Table 4.1.

Rock Magnetism

The rock magnetic experiments are preliminary checks for the suitability of the material for archaeomagnetic studies. For all sets, room temperature bulk magnetic susceptibilities and thermo-magnetic curves (Curie curves) were determined for the identification of the magnetic carriers and thermal stability. Based on the results from these experiments, additional checks including the hysteresis loop, Isothermal Remanent Magnetization (IRM) acquisition, and First Order Reversal Curve (FORC) diagram measurements were performed on nine sets that appeared suitable for archaeointensity measurements (Fig. 4.2).

The room temperature bulk magnetic susceptibilities of all samples are measured to calculate the

© BIBLIOLS PUBLISHERS
THIS DOCUMENT MAY BE PRINTED FOR PRIVATE USE ONLY
IT MAY NOT BE DISTRIBUTED WITHOUT PERMISSION OF THE PUBLISHER.

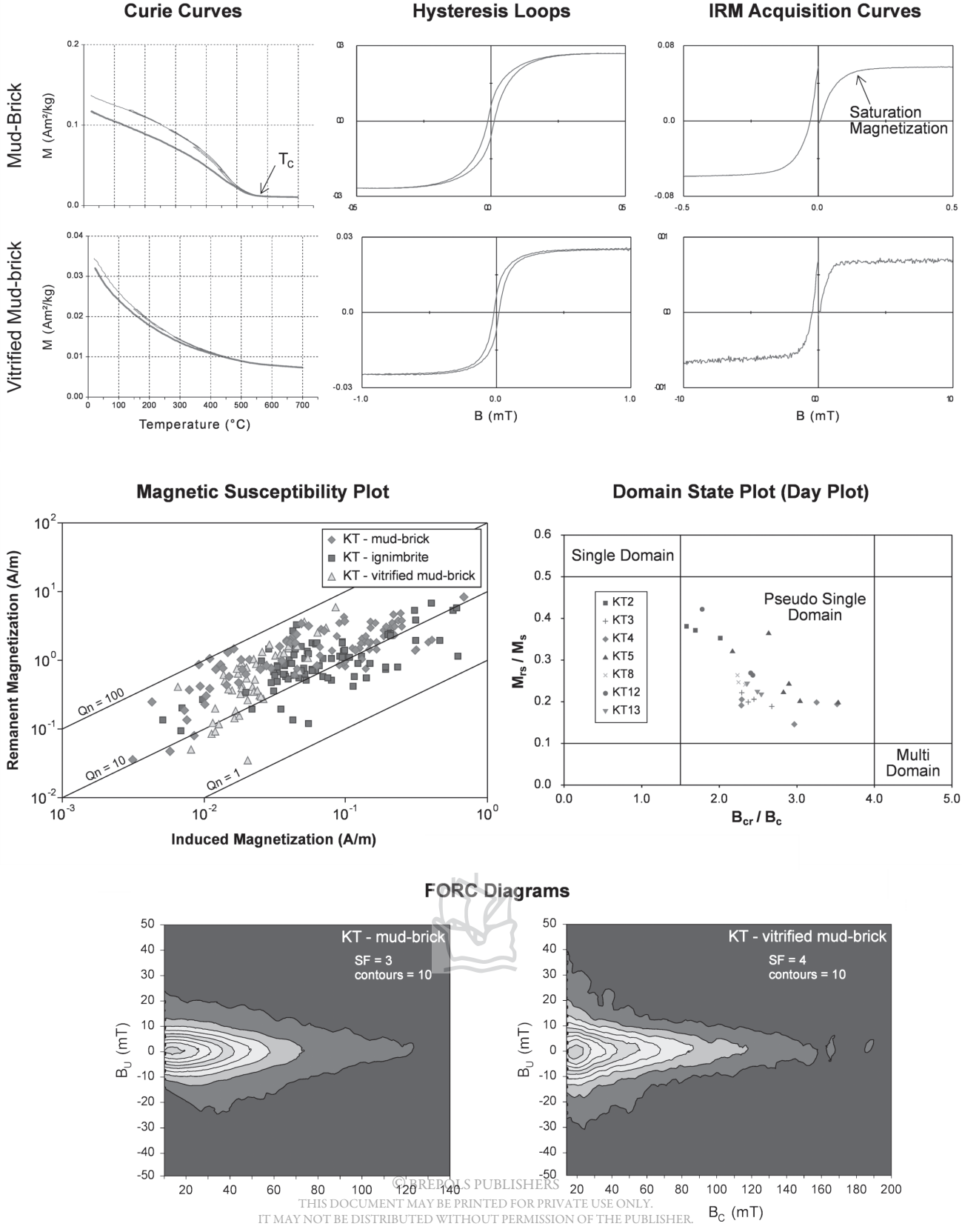

©BREPOLS PUBLISHERS
THIS DOCUMENT MAY BE PRINTED FOR PRIVATE USE ONLY.
IT MAY NOT BE DISTRIBUTED WITHOUT PERMISSION OF THE PUBLISHER.

Figure 4.2. Rock magnetic properties representative of each building material. Figures by the authors.

Koenigsberger Ratio (Q_n), which is an appropriate measure to check whether the samples carry a stable thermo-remanent magnetization (TRM) rather than a recent viscous remanent magnetization (VRM). For all three types of building materials, TRM strongly dominates (Q_n>1) providing a positive stability test.

Thermo-magnetic measurement is the primary method for the identification of the magnetic carrier since each mineral has its own Curie temperature (T_c). A single Curie point on the curve indicates the dominance of a single carrier. The difference between the cooling and heating curves indicates alteration. The experiments run on mud-bricks show magnetite magnetization with near reversible heating/cooling curves with a single Curie temperature at ~580 °C. The hyperbolic curve from the vitrified mud-brick, on the other hand, did not allow identification of the magnetic carrier. The curves from the ignimbrites have a single T_c at ~580 °C but display significant difference on heating and cooling curves indicating alteration, and therefore discarded from archaeointensity analysis.

Hysteresis loop parameters and IRM acquisition curves are helpful to specify the domain state of the magnetic mineral that is essential for archaeointensity measurements. In general, single domain (SD) particles are ideal, pseudo single domain (PSD) particles are well-behaved, and multi domain (MD) particles are problematic, as also are the minerals with high saturation fields and magnetic interactions. The results of all measurements on mud-bricks and vitrified mid-bricks show that the samples consist only of PSD grains (Day plot in Fig. 4.2),[4] and there is no indication of a high coercivity mineral in the IRM acquisition curves since all the samples are saturated in low fields below ~200 mT.

A FORC diagram is a second check for the domain state and provides additional information on the interaction fields of magnetic minerals.[5] The mud-bricks and vitrified mud-bricks have a symmetrical FORC diagram with one closed inner contour and a very narrow contour spreading along the ordinate indicating the assemblages are dominated by non-interacting PSD grains.

Demagnetization, ChRM, and Directional Results

Demagnetization

Two techniques, thermal (Th) and alternating field (AF) demagnetization, were used to measure the magnetic remanence in each sample. Thermal experiments were performed using a cryogenic magnetometer while the AF measurements were carried out on a high precision robotized cryogenic magnetometer. At least fourteen samples from each set were demagnetized with small incremental steps up to a maximum of 580 °C or 100 mT. The demagnetization results were plotted in orthogonal projection diagrams.[6] One representative diagram from each type of building material is plotted in Figure 4.3. All mud-bricks and the majority of ignimbrite samples have single component demagnetization diagrams uniformly decaying to the origin. This indicates either the primary magnetization (the NRM gained during manufacture) or, if present the secondary event (in this case the TRM recorded during fire) that caused the material to (re)gain remanent magnetization, is fully recorded. Occasionally, the demagnetization diagrams show two components pointing to 'partial burning' (meaning the samples were not heated to their Curie temperatures). In this case, the low-temperature component (marked as LT in Fig. 4.3) can be interpreted as the record from the burning event and the high-temperature (HT) component is the sample's original magnetization.

Characteristic Remanent Magnetization (ChRM) Directions

The remanent magnetization directions are interpreted via the principle component analysis.[7] The mean directions were calculated according to Fisher.[8] The acceptance criteria for maximum angular deviation (MAD) of individual directions and the α_{95} cone of confidence of the means are taken as 10 °, but values are typically much lower than that. The quality of the cluster is assessed with the dispersion parameter (k) where we require k>100. The results of directional analyses are reported in Table 4.2.

The sets that are composed solely of mud-bricks (KT1, KT2, and KT3) produced good quality demagnetization diagrams and well-defined ChRM directions with high k values (200–600) and low α_{95} (<1.7).

© BREPOLS PUBLISHERS
THIS DOCUMENT MAY BE PRINTED FOR PRIVATE USE ONLY.
IT MAY NOT BE DISTRIBUTED WITHOUT PERMISSION OF THE PUBLISHER.

[4] Day *et al.* 1977.

[5] Roberts *et al.* 2000.

[6] Zijderveld 1967.

[7] Kirschvink 1980.

[8] Fisher 1953.

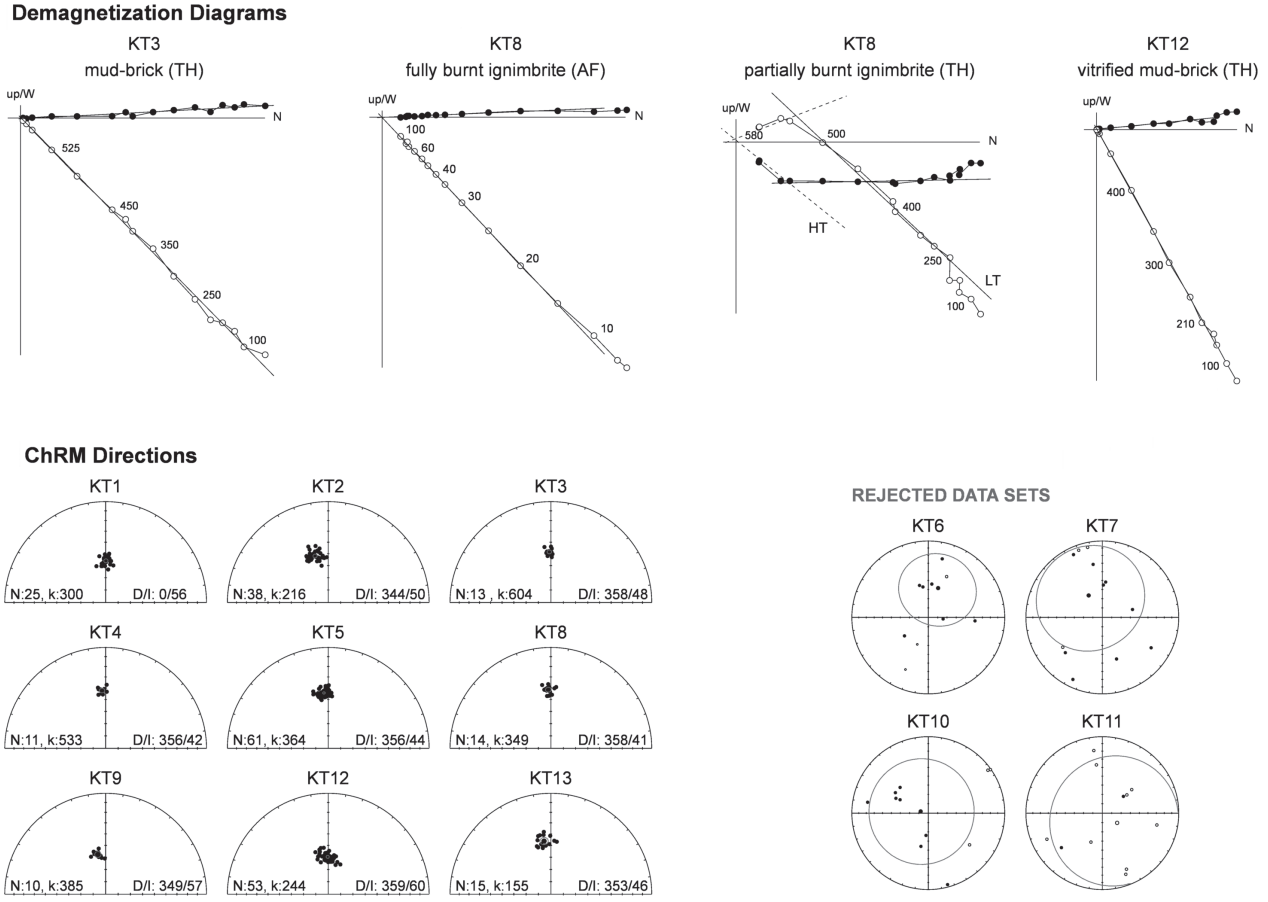

Figure 4.3. Representative examples of demagnetization diagrams of each type of building material, equal area projections of the ChRM directions of all sets, and the examples of accepted and rejected plots from three different protocols adopted in the archaeointensity experiments. LT/HT is the low-temperature/high-temperature component, N is the number of samples, *k* is the dispersion parameter and D/I is the declination/inclination. Closed (open) symbols in the demagnetization diagrams represent the projection of the vector end-points on the horizontal (vertical) plane. Figures by the authors.

© BREPOLS PUBLISHERS
THIS DOCUMENT MAY BE PRINTED FOR PRIVATE USE ONLY
IT MAY NOT BE DISTRIBUTED WITHOUT PERMISSION OF THE PUBLISHER

Table 4.2. Summary of directional results. All directions are corrected for IGRF deviation. n/N, number of samples accepted over measured; Dec, mean declination; Inc, mean inclination; k, dispersion parameter; α_{95}, 95 per cent confidence cone of mean directions. In italic are the rejected data sets due to poor cluster. Table by the authors.

Site	Treatment	n/N	Dec	Inc	k	α_{95}
KT1	Th, AF	25/26	5.0	56.0	300.0	1.7
KT2	Th, AF	38/44	-11.3	50.3	215.7	1.6
KT3	Th, AF	13/14	2.9	48.4	603.9	1.7
KT4	Th, AF	11/15	1.0	42.1	533.2	2.0
KT5	Th, AF	61/70	0.2	44.2	363.9	1.0
KT6	*Th, AF*	*NOT BURNT*				
KT7	*Th, AF*					
KT8	Th, AF	14/17	2.2	41.4	348.9	2.1
KT9	Th, AF	10/16	-6.5	57.0	385.3	2.5
KT10	*Th, AF*	*NOT BURNT*				
KT11	*Th, AF*					
KT12	Th, AF	53/53	3.9	59.7	243.7	1.3
KT13	Th, AF	15/18	-2.6	45.9	154.8	3.1

Out of five sets that are composed only of ignimbrites, the demagnetization diagrams of four sets (KT6, KT7, KT10, and KT11) are of good quality again, however, with completely random directions (the rejected sets in Fig. 4.3). The ChRM directions with no cluster indicate an insufficient burning where the samples still carry their original magnetization. The samples from the last ignimbrite set, KT9, were either fully burnt providing a meaningful direction or sufficiently heated to have a clear well-determined LT component in the demagnetization diagram that we consider representing a ChRM due to firing. This set is also of good quality with k>300, α_{95} <2.5.

There are four sets (KT4, KT5, KT8, and KT13) that are composed of both mud-bricks and ignimbrites. The ignimbrite samples from these sets have either single or two component demagnetization diagrams whereas the mud-bricks are single component. When the LT component of the ignimbrites are isolated, the directions obtained from these two different building materials become extremely consistent within each set providing well-defined ChRM directions with k>155 and α_{95} <3.1.

The oldest (Early Bronze III) set, KT12, is entirely composed of vitrified mud-bricks. The demagnetization diagrams are single component and the magnetization is completely removed at ~500 °C pointing to Titanium-poor magnetite as the carrier (where the hyperbolic Curie curves (Fig. 4.2) did not allow identification of the magnetic mineral). The set displays a well-defined ChRM with k = 244 and α_{95} = 1.3.

Out of the thirteen sets of samples from the site, four sets turned out to be not burnt. The remaining nine sets are considered to be of good quality with IGRF corrected declinations between 348.7° and 5.0° and inclinations between 41.4° and 59.7°.

Archaeointensity Experiments and Results

The Experimental Procedure

Regarding the difficulties in obtaining a reliable archaeointensity estimate (discussed in section 2), it is crucial to employ different techniques, if possible. In this study, we adopted three protocols for the archaeointensity experiments. These three methods were also applied to a large set of volcanics by de Groot[9] who concluded that the results were remarkably accurate if the results of two or more methods mutually agreed, testifying to the importance to not adhere to just one protocol. A brief description of each method is given below.

Thermal Thellier-Thellier Technique

The method developed by Thellier and Thellier[10] is based on progressively removing the NRM and replacing it with a laboratory TRM via step-wise heating. First the sample is heated to a particular temperature and then cooled to room temperature in a laboratory field, B_{lab}. Next, a second heating is performed to the same temperature and cooled down but this time in the opposite field direction ($-B_{lab}$). Vector subtraction of these two steps allows the determination of the NRM remaining at each temperature step and the partial TRM (pTRM) gained. The ancient field strength is proportional to the slope of the best fit line of NRM against pTRM.

In this study, we followed the IZZI protocol[11] which is a combination of Coe[12] and Aitken[13] modifications of the method where an in-field step is followed by a zero-field step (IZ) or vice versa (ZI). A custom-built orientation tray was used to align each sample's NRM with the applied field direction, reducing the effects of ani-

[9] De Groot *et al.* 2013.

[10] Thellier & Thellier 1959.

[11] Tauxe & Staudigel 2004; Yu *et al.* 2004.

[12] Coe 1967.

[13] Aitken 1988.

© ARCHAEOLS PUBLISHING
THIS DOCUMENT MAY BE PRINTED FOR PRIVATE USE ONLY
IT MAY NOT BE DISTRIBUTED WITHOUT PERMISSION OF THE PUBLISHER.

sotropy during TRM acquisition.[14] The acceptance criteria, adopted from Coe[15] and supplemented by those of Selkin and Tauxe[16] are as follows:

1. The number of points used for the best fit line (N) ≥5
2. The ratio of standard error of the slope to absolute value of the slope (β) <0.1
3. The NRM fraction (f) ≥0.4
4. Quality factor (q)>5, where most results are higher than 10
5. The number of successful pTRM checks ≥3
6. The ratio of difference between the pTRM check and relevant TRM value to the length of the selected NRM-TRM segment (DRAT) <10 per cent
7. MD behavior of the interpreted segment of the NRM-TRM plot is assessed by the curvature statistic, $|k|$, and the acceptance limit is taken as 0.164.[17]

Microwave Technique

As described in the previous sections, the major problem with the archaeointensity experiments is the mineral alteration caused as a result of multiple heatings. The basic principle of the method is identical with what is described in the thermal Thellier method. The only technical difference is that the excitation of electrons (hence, the heating) takes place only on magnetic minerals by means of microwaves instead of heating the whole sample which is the case for the thermal Thellier method.

We performed twenty-one microwave measurements on one to five samples from each set. Possible influence of anisotropy was checked for by comparing the direction of the magnetization acquired with that of the applied field. In all cases, no significant systematic off-sets were observed suggesting that anisotropy was negligible. To monitor thermo-chemical alteration, pTRM checks were performed after every two double-treatments. The same selection criteria were employed as in the TT experiments.

Multi-Specimen Method

To reduce the effect of non-ideal MD behaviour and progressive alteration during TT experiments,[18] Dekkers and Böhnel proposed a method, the 'multi-specimen parallel differential pTRM method', here referred to as MSP-DB. The idea behind the method is simple: to overprint an ancient TRM with a laboratory pTRM induced at a temperature much lower than the Curie temperature in a laboratory field applied in the same direction as the TRM. The initial suggestion that this protocol was domain-state independent, however, did not hold; Fabian and Leonhardt[19] proposed an addition to the protocol to correct for MD behaviour. As a rule, we apply the domain-state corrected protocol, referred to as MSP-DSC. The experiments were run on four samples from each set. The MSP experiments were accepted if the average progressive alteration, ε_{alt} <3 per cent. For the MSP-DCS protocol there is an additional requirement where, Db, the difference between the theoretical (b =-1) and the actual value of y-axis intercept of the best-fit line should be smaller than 10 per cent. If this requirement was not fulfilled, implying that the MSP-DSC protocol did not properly correct for MD behaviour, we used the MSP-DB protocol provided that the ε_{alt} is still less than 3 per cent.

Archaeointensity Results

The measurements were carried out on eight sets (one set of vitrified mud-brick and seven mud-brick sets) out of thirteen. In addition, from set KT3, three microwave measurements were performed on sherds. Four sets (KT6, KT7, KT10, and KT11) were discarded based on their directional results and one ignimbrite set (KT9) due to its rock magnetic properties. Five sets successfully yielded a result in all three methods. Figure 4.3 shows an example of a successful and a failed measurement from each method and the results are reported in Table 4.3. Out of forty-nine TT and MW measurements, forty were successful yielding a success rate of 82 per cent. From eight sets of MSP measurements, seven were successful either with DSC or DB solution. The results from different protocols reasonably agree with each other and no systematic differences were observed between the TT and MW results from the same sample sets. For the samples of same origin, if the cooling rate effects are present, it is expected to be enhanced

© BREPOLS PUBLISHERS
THIS DOCUMENT MAY BE PRINTED FOR PRIVATE USE ONLY
IT MAY NOT BE DISTRIBUTED WITHOUT PERMISSION OF THE PUBLISHER.

[14] Rogers *et al.* 1979.

[15] Coe *et al.* 1978.

[16] Selkin & Tauxe 2000.

[17] Paterson 2011.

[18] Dekkers & Böhnel 2006.

[19] Fabian & Leonhardt 2010.

Table 4.3. The intensity results obtained from three protocols. N/n, number of samples measured over accepted; PI, paleointensity; A, the average paleointensity value of individual samples; stdev, the standard deviation. Table by the authors.

	TT			MW			MSP				AVERAGE PI	
	N/n	PI	stdev	N/n	PI	stdev	N/n	Protocol	PI	stdev	A	stdev
KT1	1/0	-	-	1/1	60.94	-	4/4	MSP-DB	58.23	0.03	59.59	1.92
KT2	2/1	60.37	-	2/0	-	-	-	-	-	-	60.37	-
KT3	4/3	54.92	1.16	5/5	63.08	13.31	4/4	MSP-DB	40.15	0.05	57.81	12.18
KT4	5/5	55.27	4.47	1/0	-	-	4/4	MSP-DSC	51.68	0.29	54.67	4.26
KT5	4/4	49.51	7.87	3/3	56.71	2.95	4/3	MSP-DSC	43.67	0.02	51.48	7.19
KT8	7/7	53.54	0.96	3/1	56.80	-	4/3	MSP-DB	57.22	0.00	54.31	1.75
KT12	4/4	63.83	5.17	1/1	60.60	-	4/4	MSP-DB	57.66	0.07	62.26	4.78
KT13	3/3	53.38	1.38	3/2	58.20	6.30	4/3	MSP-DSC	46.92	0.03	53.91	5.10

in MW estimates and make them systematically higher than thermal estimates that use longer cooling times.[20] The agreement in TT and MW results suggests that no cooling rate correction is required for the data as a whole. Moreover, the remanence in the samples is predominantly carried by PSD grains (Fig. 4.2) for which the cooling rate effect on (p)TRM magnitude has been experimentally verified as small.[21]

From the mud-brick set KT1, we made one TT measurement which has failed and one MW measurement in which the MSP-DB result obtained from four data points is in line with the value within 5 per cent.

The samples from KT2 and KT4 produced good quality TT results, however, failed in all MW experiments either due to noisy NRM-TRM plot, indestructible NRM or MD behaviour. We were not able to perform the MSP method on KT2 because there were not enough samples, so we present an intensity value based on one TT measurement. The MSP result from KT4 is of good quality with minor alteration and Db <10 per cent allowing to opt for the domain corrected solution.

The majority of TT and MW measurements from the sets KT3 (mud-bricks and sherds), KT5, KT8, KT13 (mud-bricks), and KT12 (vitrified mud-bricks) have passed the selection criteria, producing high quality NRM-TRM plots. The samples from KT5 produced two low and two high TT results in which the lower values are in line with the MSP-DSC result and the higher values are in agreement with the MW results. Among all sets, KT8 has the most consistent results in both individual sample level and mean intensities obtained using all three protocols. The measurements from the vitrified mud-bricks of KT12 produced the highest intensity value calculated from three protocols. The samples from KT13 produced well behaved NRM-TRM plots from TT and acceptable results from MW and MSP methods.

The intensity results obtained from forty successful measurements using three protocols range between 51.48 and 62.26 μT.

Discussion

Evaluation of Directions and Intensity Results

The directional results from this study, corrected for local declination at the time of sampling, are relocated to Kayseri as the approximate centre of Turkey (lat: 38.851 °N, long: 35.631 °E), and plotted against the data from GEOMAGIA50.v3.2[22] (downloaded on December 2018 from the countries within ~1600 km radius), and the global geomagnetic field models SHA.DIF.14k and pfm9k.1b calculated at Kayseri (Fig. 4.4a).

A first observation is that the model SHA.DIF.14k fits very well with both our earlier directional observations and the results from this study, including the large declination swing to nearly 20 °E around 2000 BC (Fig. 4.4a), that was not detected by earlier models. Nor is it recorded by the heavily smoothed pfm9k.1b model. The inclination values of the sets are shallower than the model predictions by some 10° but in line with the general trend of the model. By their nature, field models are usually considerably smoother than the actual field

© BREPOLS PUBLISHERS
THIS DOCUMENT MAY BE PRINTED FOR PERSONAL USE ONLY
IT MAY NOT BE DISTRIBUTED WITHOUT PERMISSION OF THE PUBLISHER

[20] Poletti *et al.* 2013.

[21] For example: Biggin *et al.* 2013; de Groot *et al.* 2013; Yu 2011.

[22] Brown *et al.* 2015.

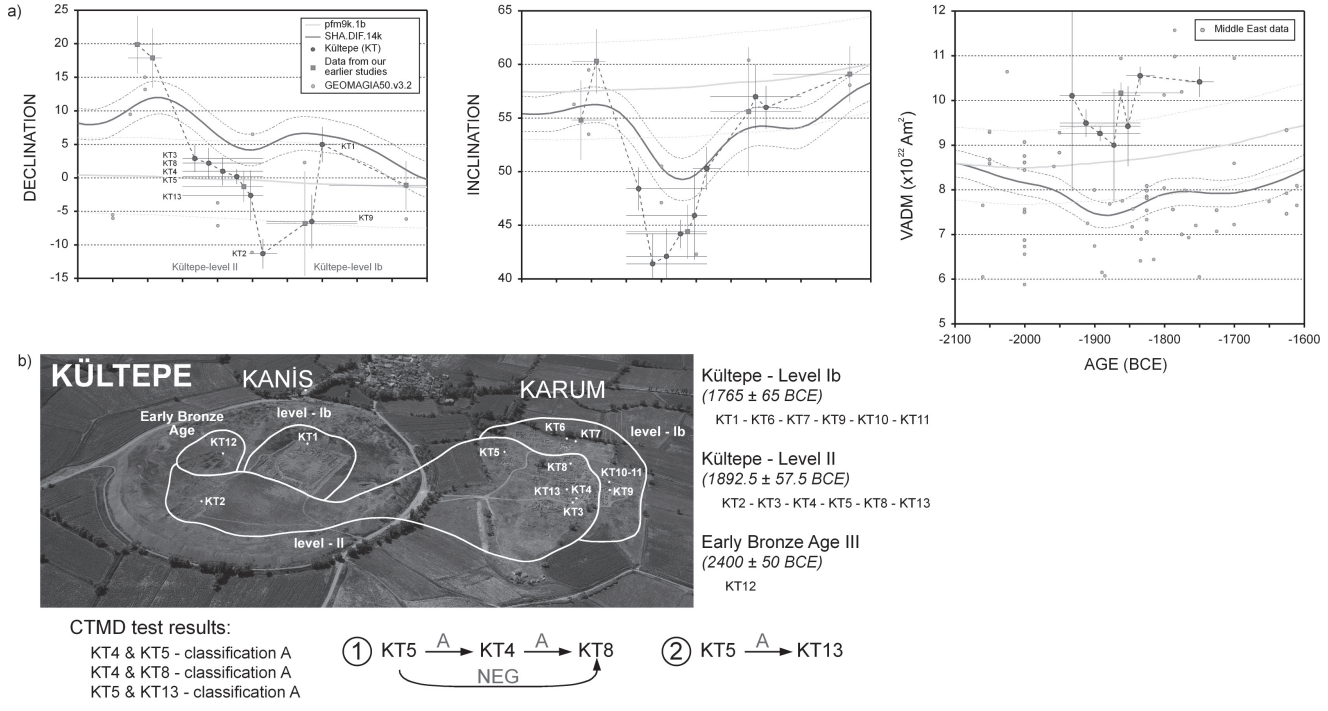

Figure 4.4. (a) Declination, inclination, and VADM distribution of Kültepe data points (large circles) as sorted from the most westerly to the most easterly declination based on the westerly trend in the SHA.DIF.14k model for the period of ~2100–1850 BC. The squares are data points from various sites in Turkey from our earlier studies and the small circles are data from GEOMAGIA.v3.2. The time intervals between sites in Kültepe-level II are arbitrarily taken as twenty years; (b) the CTMD results and areal distribution of fire events shown on an aerial photograph of Kültepe. Photos and figures by the authors.

observations. Hence, these new results are very useful to improve the resolution of the models since there is a lack of directional data for this time period. Only sixteen records are available in GEOMAGIA50.v3.2 for the seven-hundred-year period 2200–1500 BC, from Greece to Azerbaijan, and from Moldavia/Ukraine to Egypt. Our nine (out of thirteen) new directional records in this time interval plus earlier results almost double the database for this entire region. In addition, these high quality data sets contribute in terms of a better spatial distribution. This will reduce any bias (the local variations in the field) introduced by the few existing data sets, considering that the majority of the GEOMAGIA50.v3.2 data is coming from Eastern Europe, some from the Near East, and very few from the Middle East.

From a total of forty-nine TT and MW measurements, forty were successful, yielding a success rate of 83 per cent which is exceptionally high regarding the overall rate of Thellier type archaeointensity experiments. The results are coherent between samples and methods. Although the cooling rate experiment was not performed, the agreement between microwave (cool-

© BREPOLS PUBLISHERS
THIS PDF IS PRINTED FOR PRIVATE USE ONLY
IT MAY NOT BE DISTRIBUTED WITHOUT PERMISSION OF THE PUBLISHER

ing time of 10–100 seconds) and thermal Thellier-type experiment's (cooling time of 10–100 minutes) results suggest that the cooling rate effects are minimal.

To be able to make a valid comparison with the existing data (GEOMAGIA.v3.2) and the global field models (SHA.DIF.14k and pfm9k.1b), the intensity results are converted into virtual axial dipole moments (VADM).

Our data from the period 2600–1700 BC (including those of our earlier study) are always significantly higher than predicted by the SHA.DIF.14k model based on archaeomagnetic and lava flow data, and generally higher than predicted by pfm9k.1b (Fig. 4.4a) but they are not in disagreement with published data[23] that support the existence of short-lived periods with high intensities, at least as observed in the Levant.

Relative Chronology of Fire Events in Kültepe

We have analysed the directional results of Kültepe to determine if they can be attributed to the same distribution or not. This allows us to assess whether the fire events at the site belong to a single big catastrophic event or to different (temporal) events. We used the common true mean direction (CTMD) test developed by McFadden and McElhinny.[24] The test is classified as A, B, C, or indeterminate.

The sets KT4 & KT5, KT4 & KT8, and KT5 & KT13 share a CTMD with classification A. The rest of the correlations are negative. Based on the results of Kültepe-level II, the areal distribution of fires is plotted in Figure 4.4b. As can be seen from the figure, KT2, KT3, and KT9 are from local fires whereas KT4 & KT8 and KT5 & KT13 are from larger scale fires. Therefore, we can conclude that the ages of fires in Kültepe are different and the site was not abandoned as a result of a big catastrophic fire event as was previously suggested by Sagona and Zimansky.[25]

To establish a relative chronology for the fire events in Kültepe-level II (KT2, KT3, KT4, KT5, KT8, KT9, and KT13), we sorted the data based on their CTMD results and then on easternmost to westernmost declination. This best reflects the trend in the SHA.DIF.14k model at this time interval (Fig. 4.4a). In this scenario, the oldest/youngest age — within the age errors — is assigned to the most westerly/easterly declination while the time span between each fire event is arbitrarily divided into equal time intervals of twenty years. The corresponding inclination values agree fairly well with the trend of the model but in this scenario declinations are more westerly towards ~1850 BC while inclinations are steepest around 1900 BC. Although we have 'smoothed' the directional changes by shifting the results within the time span allowed by the dating error, it seems that the model has not (yet) enough resolution to predict these short-term swings in directions. The magnitude and timing of these swings are however compatible with observations of secular variation over the past three thousand years.

The VADM trend is not helpful in discriminating the best possible sequence since values are very similar. They are essentially in accordance with the trend of the curve from the SHA.DIF.14k model but systematically higher, and they are largely in agreement with pfm9k.1b. Nevertheless, the scenario preferred here represents the most reasonable sequence of fire events at Kültepe, where the rate of directional variations is similar to secular variation as observed today. We do realize however that other scenarios are possible, and that the time constraints within the given age uncertainty do not allow this — or any other — scenario to be robust. For example, a scenario in which the data sets are sorted on increasing inclinations based on the mild increasing trend in the model, results in more abrupt changes compared to the first scenario, and the declinations display erratic jumps of 5–15° within ten-year time intervals. We favour the scenario outlined above (Fig. 4.4a) in which both declination and inclination change gradually and abrupt and unlikely erratic changes in the directions in such a short time interval are avoided.

Timing of Tilting of the Wall in Ilemma House

Among our sampling sets, one set was collected from a tilted mud-brick wall and its intact ignimbrite foundation stones (Fig. 4.1, KT8 samples from Ilemma House). As the acquisition of magnetization takes place during cooling, by analysing the directional results with and without a tilt correction (which is restoring the wall's present orientation to its original position), it is possible to determine if the tilting has occurred during the fire or long after. When the directions from KT8 are assessed with and without a tilt correction, the results

© BREPOLS PUBLISHERS
THIS DOCUMENT MAY BE PRINTED FOR PERSONAL USE ONLY
IT MUST NOT BE MODIFIED OR REDISTRIBUTED WITHOUT PERMISSION OF THE PUBLISHER

[23] For example: Ben-Yosef *et al.* 2009; Ertepinar *et al.* 2012; Shaar *et al.* 2011; Ertepinar *et al. submitted*.

[24] McFadden & McElhinny 1990.

[25] Sagona & Zimansky 2009.

are coherent with the expected directions and the directions from the ignimbrites only without a tilt correction, implying that the tilting — the collapse of the wall — must have occurred during the fire event.

Conclusions

This study concentrated on untangling the fire events in Kültepe. Not solely directions or intensities but the characterization of the full vector field is required for the most accurate interpretation. To assure that our samples are suitable for directional and intensity experiments, we first tested the rock magnetic properties and verified that most of the samples have ideal behaviour. The conclusions can be summarized as follows:

1. The directional results are highly coherent with the existing data in the literature and the global field model SHA.DIF.14k but the intensities are significantly higher than the model predictions.
2. The foundation part of a structure is not sufficiently heated, therefore, not ideal for archaeomagnetic studies.
5. The ignimbrites with two component demagnetization diagrams are heated up to a maximum temperature of 500 °C.
4. The collapse of the mud-brick wall in Ilemma House must have occurred during the fire event.
5. Based on the CTMD results, we propose that the timings of fire events are different and the abandonment of the site was not the result of a single catastrophic fire event.

Acknowledgements

We would like to thank the late Prof. Dr Kutlu Emre for her valuable feedback about Kültepe. We are also grateful to people in the excavation team who were helpful at all times. Particular thanks are due to Nuretdin Kaymakci, the drilling expert on fragile archaeological material.

Bibliography

Aitken, Michael J.; Allsop, A. L.; Bussell, G. D. & Winter, M. B.
1988 'Determination of the Intensity of the Earth's Magnetic Field during Archaeological Times: Reliability of the Thellier Technique', *Reviews of Geophysics* 26: 3–12.

Ben-Yosef, Erez; Tauxe, Lisa; Levy, Thomas E.; Shaar, Ron; Ron, Hagai & Najjar, Mohammad
2009 'Geomagnetic Intensity Spike Recorded in High Resolution Slag Deposit in Southern Jordan', *Earth and Planetary Science Letters* 287: 529–39, doi:10.1016/j.epsl.2009.09.001.

Biggin, Andrew J.; Badejo, S.; Hodgson, Emma; Muxworthy, Adrian R.; Shaw, J. & Dekkers, Mark J.
2013 'The Effect of Cooling Rate on the Intensity of Thermoremanent Magnetization (TRM) Acquired by Assemblages of Pseudo-Single Domain, Multidomain and Interacting Single-Domain Grains', *Geophysical Journal International* 193: 1239–49, doi:10.1093/gji/ggt078.

Brown, Maxwell C.; Donadini, Fabio; Korte, Monika; Nilsson, Andreas; Korhonen, Kimmo; Lodge, Alexandra; Lengyel, Stacey N. & Constable, Catherine G.
2015 'GEOMAGIA50.v3: 1. General Structure and Modifications to the Archeological and Volcanic Database', *Earth, Planets and Space* 67: 83.

Coe, Robert S.
1967 'Paleo-Intensities of the Earth's Magnetic Field Determined from Tertiary and Quaternary Rocks', *Journal of Geophysical Research* 72: 3247–62, doi:10.1029/JZ072i012p03247.

© BREPOLS PUBLISHERS
THIS DOCUMENT MAY BE PRINTED FOR PRIVATE USE ONLY.
IT MAY NOT BE DISTRIBUTED WITHOUT PERMISSION OF THE PUBLISHER.

Coe, Robert S.; Grommé, Sherman & Mankinen, Edward A.
1978 'Geomagnetic Paleointensities from Radiocarbon-Dated Lava Flows on Hawaii and the Question of the Pacific Nondipole Low', *Journal of Geophysical Research* 83: 1740–56, doi:10.1029/JB083iB04p01740.

Day, Ron W.; Fuller, Michael & Schmidt, Victor A.
1977 'Hysteresis Properties of Titanomagnetites: Grain-Size and Compositional Dependence', *Physics of the Earth and Planetary Interiors* 13: 260–67.

de Groot, Lennart V.; Biggin, Andrew J.; Dekkers, Mark J.; Langereis, Cornelis G. & Herrero-Bervera, Emilio
2013 'Rapid Regional Perturbations to the Recent Global Geomagnetic Decay Revealed by a New Hawaiian Record', *Nature Communications* 4: 2727, doi:10.1038/ncomms3727.

Dekkers, Mark J. & Böhnel, Harald N.
2006 'Reliable Absolute Palaeointensities Independent of Magnetic Domain State', *Earth and Planetary Science Letters* 248: 508–17.

Ertepinar, Pinar; Langereis, Cor G.; Biggin, Andrew J.; Frangipane, Marcella; Matney, Timothy; Ökse, Tuba & Engin, Atilla
2012 'Archaeomagnetic Study of Five Mounds from Upper Mesopotamia between 2500 and 700 BCE: Further Evidence for an Extremely Strong Geomagnetic Field *ca.* 3000 Years Ago', *Earth and Planetary Science Letters* 357/58: 84–98.

Ertepinar, Pinar; Hammond, Megan L.; Hill, Mimi J.; Biggin, Andrew J.; Langereis, Cor G.; Herries, A. I. R.; Yener, K. Aslıhan; Akar, Murat; Yazicioglu, Gökçe B.; Gates, Mary; Harrison, Timothy; Frankel, D.; Webb, J. M.; Greaves, Alan M. & Ozgen, Ilknur
2019 'Archaeomagnetic Records from Mediterranean Settlements', submitted to: *Earth and Planetary Science Letters*.

Fabian, Karl & Leonhardt, Roman
2010 'Multiple-Specimen Absolute Paleointensity Determination: An Optimal Protocol including pTRM Normalization, Domain-State Correction, and Alteration Test', *Earth and Planetary Science Letters* 297: 84–94, doi:10.1016/j.epsl.2010.06.006.

Fisher, Ronald A.
1953 'Dispersion on a Sphere', *Proceedings of the Royal Society of London* 217A: 295–305.

Kirschvink, Joseph L.
1980 'The Least-Squares Line and Plane and the Analysis of Palaeomagnetic Data', *Geophysical Journal of the Royal Astronomical Society* 62: 699–718, doi:10.1111/j.1365–246X.1980.tb02601.x.

McFadden, Philip L. & McElhinny, Michael W.
1990 'Classification of the Reversal Test in Palaeomagnetism', *Geophysical Journal International* 103: 725–29, doi:10.1111/j.1365–246X.1990.tb05683.x.

Nilsson, Andreas; Holme, Richard; Korte, Monika; Suttie, Neil & Hill, Mimi
2014 'Reconstructing Holocene Geomagnetic Field Variation: New Methods, Models and Implications', *Geophysical Journal International* 198: 229–48.

Paterson, Greig A.
2011 'A Simple Test for the Presence of Multidomain Behavior during Paleointensity Experiments', *Journal of Geophysical Research: Solid Earth* 116: 1–12, doi:10.1029/2011JB008369.

Pavon-Carrasco, Francisco Javier; Osete, Maria Luisa; Torta, Joan Miquel & De Santis, Angelo
2014 'A Geomagnetic Field Model for the Holocene Based on Archaeomagnetic and Lava Flow Data', *Earth and Planetary Science Letters* 388: 98–109.

© BREPOLS PUBLISHERS
THIS DOCUMENT MAY BE PRINTED FOR PRIVATE USE ONLY.
MAY NOT BE DISTRIBUTED WITHOUT PERMISSION OF THE PUBLISHER.

Poletti, Wilbor; Hartmann, Gelvam A.; Hill, Mimi J.; Biggin, Andrew J. & Trindade, Ricardo I. F.
2013 'The Cooling-Rate Effect on Microwave Archeointensity Estimates', *Geophysical Research Letters* 40: 3847–52, doi:10.1002/grl.50762.

Roberts, Andrew P.; Pike, Christopher R. & Verosub, Kenneth L.
2000 'First-Order Reversal Curve Diagrams: A New Tool for Characterizing the Magnetic Properties of Natural Samples', *Journal of Geophysical Research* 105: 461–76, doi:10.1029/2000JB900326.

Rogers, John B.; Fox, Julianne M. W. & Aitken, Melissa J.
1979 'Magnetic Anisotropy in Ancient Pottery', *Nature* 277: 644–46.

Sagona, Antonio G. & Zimansky, Paul E.
2009 *Ancient Turkey* (Routledge World Archaeology), 1st edn. Routledge, London.

Selkin, Peter A. & Tauxe, Lisa
2000 'Long-Term Variations in Palaeointensity', *Philosophical Transactions of the Royal Society of London*, ser. A: *Mathematical Physical and Engineering Sciences* 358: 1065–88, doi:10.1098/rsta.2000.0574.

Shaar, Ron; Ben-Yosef, Erez; Ron, Hagai; Tauxe, Lisa; Agnon, Amotz & Kessel, Ronit
2011 'Geomagnetic Field Intensity: How High Can It Get? How Fast Can It Change? Constraints from Iron Age Copper Slag', *Earth and Planetary Science Letters* 301: 297–306, doi:10.1016/j.epsl.2010.11.013.

Shaar, Ron; Tauxe, Lisa; Ron, Hagai; Ebert, Yael; Zuckerman, Sharon; Finkelstein, Israel & Agnon, Amotz
2016 'Large Geomagnetic Field Anomalies Revealed in Bronze to Iron Age Archeomagnetic Data from Tel Megiddo and Tel Hazor, Israel', *Earth and Planetary Science Letters* 442: 173–85, doi:10.1016/j.epsl.2016.02.038.

Tauxe, Lisa & Staudigel, Hubert
2004 'Strength of the Geomagnetic Field in the Cretaceous Normal Superchron: New Data from Submarine Basaltic Glass of the Troodos Ophiolite', *Geochemistry, Geophysics, Geosystems* 5, doi:10.1029/2003GC000635.

Thellier, Emile & Thellier, Odette
1959 'Sur l'intensité du champ magnétique terrestre dans le passé historique et geologique', *Annals of Geophysics* 15: 285–378.

Yu, Yongjae
2011 'Importance of Cooling Rate Dependence of Thermoremanence in Paleointensity Determination', *Journal of Geophysical Research: Solid Earth* 116, doi:10.1029/2011JB008388.

Yu, Yongjae; Tauxe, Lisa & Genevey, Agnès
2004 'Toward an Optimal Geomagnetic Field Intensity Determination Technique', *Geochemistry, Geophysics, Geosystems* 5, doi:10.1029/2003GC000630.

Zijderveld, J. D. A.
1967 'A. C. Demagnetization of Rocks: Analysis of Results', in David W. Collinson, Kenneth M. Creer & Stanley K. Runcorn (eds), *Methods in Palaeomagnetism*. Elsevier, Amsterdam: 254–86.

© BREPOLS PUBLISHERS
THIS DOCUMENT MAY BE PRINTED FOR PRIVATE USE ONLY.
IT MAY NOT BE DISTRIBUTED WITHOUT PERMISSION OF THE PUBLISHER.